







Perturbations in stratospheric aerosol evolution due to the water-rich plume of the 2022 Hunga-Tonga eruption

Yunqian Zhu^{1,2,3}[✉], Charles G. Bardeen¹, Simone Tilmes¹, Michael J. Mills¹, Xinyue Wang¹, V. Lynn Harvey², Ghassan Taha^{4,5}, Douglas Kinnison¹, Robert W. Portmann⁶, Pengfei Yu⁷, Karen H. Rosenlof⁶, Melody Avery^{3,8}, Corinna Kloss⁹, Can Li^{5,10}, Anne S. Glanville¹, Luis Millán¹¹, Terry Deshler², Nickolay Krotkov⁵ & Owen B. Toon^{2,12}

The January 2022 Hunga Tonga-Hunga Ha'apai volcanic eruption injected a relatively small amount of sulfur dioxide, but significantly more water into the stratosphere than previously seen in the modern satellite record. Here we show that the large amount of water resulted in large perturbations to stratospheric aerosol evolution. Our climate model simulation reproduces the observed enhanced water vapor at pressure levels ~30 hPa for three months. Compared with a simulation without a water injection, this additional source of water vapor increases hydroxide, which halves the sulfur dioxide lifetime. Subsequent coagulation creates larger sulfate particles that double the stratospheric aerosol optical depth. A seasonal forecast of volcanic plume transport in the southern hemisphere indicates this eruption will greatly enhance the aerosol surface area and water vapor near the polar vortex until at least October 2022, suggesting that there will continue to be an impact of this eruption on the climate system.

¹Atmospheric Chemistry Observations and Modeling Laboratory, National Center for Atmospheric Research, Boulder, USA. ²Laboratory for Atmospheric and Space Physics, University of Colorado Boulder, Boulder, USA. ³University of Colorado Cooperative Institute for Research in Environmental Sciences (CIRES) at the NOAA Chemical Sciences Laboratory, Boulder, CO, USA. ⁴GESTAR II, Morgan State University, Baltimore, USA. ⁵Goddard Space Flight Center, National Aeronautics and Space Administration, Greenbelt, USA. ⁶Chemical Sciences Laboratory, National Oceanic and Atmospheric Administration, Boulder, CO, USA. ⁷Institute for Environmental and Climate Research, Jinan University, Guangzhou, China. ⁸NASA Langley Research Center, Hampton, VA, USA. ⁹Laboratoire de Physique et Chimie de l'Environnement et de l'Espace, CNRS UMR 7328, Université d'Orléans, Orléans, France. ¹⁰Earth System Science Interdisciplinary Center, University of Maryland, College Park, USA. ¹¹Jet Propulsion Laboratory, California Institute of Technology, Pasadena, CA, USA. ¹²Department of Atmospheric and Oceanic Sciences, University of Colorado Boulder, Boulder, USA. ✉email: yunqian.zhu@colorado.edu

On January 13 and 15 of 2022, the Hunga Tonga-Hunga Ha'apai (HTHH) submarine volcano (21°S, 175°W) erupted and injected volcanic material into the stratosphere up to an altitude of 58 km^{1–3}. Observations from several satellites showed enhanced levels of stratospheric sulfur dioxide (SO₂) (by the TROPOspheric Monitoring Instrument, TROPOMI and the Ozone Mapping and Profiling Suite Nadir-Mapper, OMPS-NM), water vapor (by the Microwave Limb Sounder, MLS), aerosols (by OMPS Limb Profiler, OMPS LP and Cloud-Aerosol Lidar with Orthogonal Polarization, CALIOP), and possibly ice (by CALIOP) as we will discuss in this work. Unlike some land-based volcanos, HTHH injected more than 100 Tg of water into the stratosphere^{4,5}, which normally contains about 1500 Tg of water globally defined for a tropopause pressure of 100 hPa. The MLS onboard NASA's Earth Observing System (EOS) Aura satellite⁶ observed enhanced water vapor that persisted for more than 3 months. The CALIOP on the Cloud-Aerosol Lidar and Infrared Pathfinder Satellite Observation (CALIPSO) satellite⁷ observed two distinct aerosol types on January 16 after the eruption: one with weak 532 nm depolarization indicating spherical particles (such as sulfate aerosol) above 20 km, and layers at lower altitudes with large depolarization indicating particles with nonspherical shapes (such as volcanic ash and ice) (Supplementary Fig. 1). It is typical to see ice and ash immediately after an eruption (i.e., ref. ⁸). However, it is surprising to see abundant sulfate aerosol with large extinction/backscatter coefficients so quickly because SO₂ usually takes more time to be oxidized and for sulfuric acid (H₂SO₄) to nucleate into sulfate aerosol⁹.

Stratospheric water vapor and volcanic aerosols are important to both chemistry^{10–15} and radiative balance^{16–19}. Here, we demonstrate that enhanced H₂O promotes faster sulfate aerosol formation in the stratosphere leading to larger particles and larger aerosol optical depth. The water vapor injection and a small amount of evaporating ice deposits substantial water vapor in the stratosphere. Large water vapor abundances result in the formation of hydroxide (OH) which acts to speed up the conversion of SO₂ to H₂SO₄. Because of the faster formation and coagulation of sulfate aerosol, particles form with larger sizes and hence larger extinction than the ones without water injection. Finally, we predict the water vapor and aerosols that get transported toward the South Pole will linger near the polar vortex until at least October 2022.

Results

Both water injection and evaporating ice determine the water vapor remaining in the stratosphere. Here we use the Whole Atmosphere Community Climate Model (WACCM) to simulate the persistent water vapor enhancement from 10 to 50 hPa observed by MLS version 4 (Fig. 1a) from February to April. Zonal averages of simulated water vapor on March 1 shows good agreement with MLS observations (Supplementary Fig. 2). Figure 1a shows both the model (solid line) and MLS (dashed line) display a positive water vapor anomaly of 6–8 ppmv peaking at 30 hPa from February to April. The anomaly is averaged from 30°S to 0° and calculated using February, March, and April profiles minus the profile on January 5. The simulation has wider vertical extent and slightly smaller peak anomalies in March and April. Both the model and MLS (Fig. 1a) show that the positive water vapor anomaly slowly ascends from February 10 to April 1, which is largely related to the ascending branch of Brewer-Dobson circulation²⁰ (Supplementary Fig. 2b).

To be consistent with the MLS water anomalies⁵, we need to inject ~150 Tg of water in an area of ~6 × 10⁵ km², which is about three times larger than the anvil size observed by NOAA's Geostationary Operational Environmental Satellite 17 on January 15, 2022. This large area is needed because the residual amount of water is determined by the ice vapor pressure curve as shown in Supplementary Fig. 3. If we inject the water into a smaller area, the model forms too much ice and cannot retain enough water at 30 hPa as observed. It is not unreasonable to inject in a larger area. MLS observations on Jan 16 (a day after the eruption) show the latitudinal spreading of water vapor anomaly is more than 10 degrees⁵. The simulated plume does not spread as fast as observed because it is hard for the global model to reproduce the vertical wind shear as observed due to the limited spatial resolution, especially for a tropical volcanic plume spreading in the first couple of days²¹. In the model, the injection is over 6 h on January 15, 2022 between 25.5 and 35 km with a majority of the water injected between 25.5 and 30 km (see Methods for details). The model simulation (Fig. 1b) shows that 10 Tg of ice falls out and 10 Tg of ice evaporates and contributes to the residual water vapor (~140 Tg) until April. In actuality, it is possible that more H₂O was injected and formed ice particles, but these ice particles may have fallen out because of their large size, or because they aggregated with ash particles⁸.

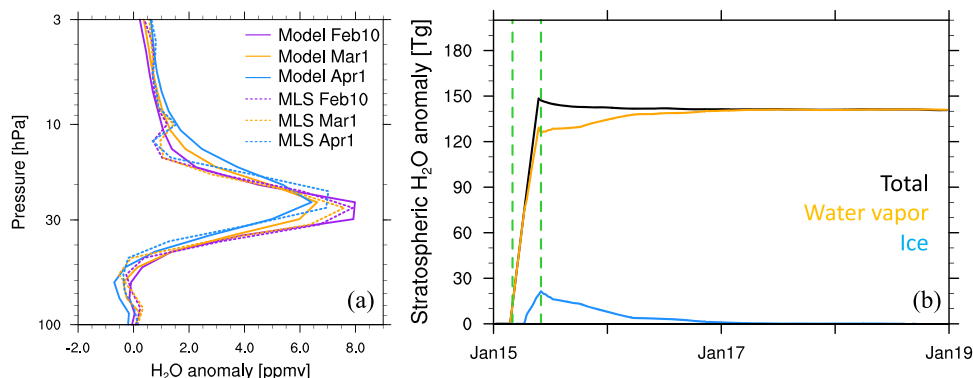


Fig. 1 The H₂O (water) profile and evolutions after the Hunga Tonga-Hunga Ha'apai eruption. **a** The zonal average H₂O anomaly profiles between 30°S–0° on February 10, March 1, and April 1, 2022. The solid lines are simulations and the dashed lines are the MLS observations. The simulation and MLS anomaly curves are calculated using February, March, and April profiles minus the profile on January 5. **b** Simulated stratospheric H₂O anomaly evolution in the first week. It is calculated using a case with H₂O injection minus a case without H₂O injection. The blue line is the ice, the orange line is the water vapor, and the black line is the total water. The green dashed lines indicate the water injection period.

The water injection significantly shortens the SO₂ lifetime by providing abundant OH. An accurate volcanic SO₂ lifetime is key for predicting the particle sizes in the volcanic cloud. With shorter lifetimes, the resulting aerosol concentration is higher, leading to more rapid coagulation and larger sulfate particles²². In the stratosphere, the volcanic SO₂ lifetime is mainly determined by its reaction rate with OH, as well as the heterogeneous reaction on ash²¹. The depletion of OH in SO₂-rich plumes slows the SO₂/OH reaction^{9,21,23–25}. However, during the HTHH eruption, the notable amount of water vapor injected rapidly increased OH¹⁵ (Supplementary Fig. 4) and shortened the SO₂ lifetime as shown in Fig. 2. The simulated SO₂ (blue dash line) is within the observational error bars (i.e., uncertainty of 35% and 30%²⁶ for

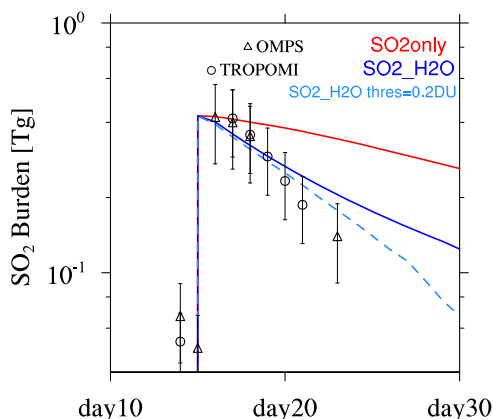


Fig. 2 The time series of the stratospheric SO₂ (sulfur dioxide) burden.

The blue and red lines are two model cases with and without water injection. The dashed blue line is the SO₂_H₂O case excluding the SO₂ below 0.2 DU (i.e., the approximate OMPS-NM (the Ozone Mapping and Profiling Suite Nadir-Mapper) SO₂ detection limit). The circles and triangles are SO₂ measurements by OMPS-NM and TROPOMI (the TROPospheric Monitoring Instrument). The error bars imply an estimated uncertainty of 35% and 30%²⁶ for OMPS-NM and TROPOMI SO₂ mass estimates, respectively. The observational data are from <https://so2.gsfc.nasa.gov/>. The SO₂only run has the SO₂ injection; the SO₂_H₂O run has both the SO₂ and H₂O injections (detailed in Online methods).

OMPS-NM and TROPOMI SO₂ mass estimates, respectively). Clegg and Abbatt²⁷ demonstrated that SO₂ uptake on the ice surfaces is insignificant, so this mechanism is not included in the model. The SO₂ lifetime (the e-folding time) of the SO₂only case (red line) is 28 days, while the SO₂ lifetime of the SO₂_H₂O case (blue solid line) is 12 days. Previous study²¹ showed that a considerable amount of SO₂ might be undetectable because it falls below the detection limits of the instruments as it spreads through the atmosphere. However, the blue dashed line in Fig. 2 suggests that this effect is small for this eruption for the first 10 days.

Enhanced water vapor impacts the stratospheric aerosol optical depth and radiation.

We compare the stratospheric aerosol optical depth (sAOD) between OMPS-LP data and two model cases at near-infrared in Fig. 3, because the extinction coefficient retrieval near-infrared has the best accuracy among all the wavelength for the OMPS-LP instrument²⁸. Here we present the SO₂only and H₂O_SO₂ cases based on our best knowledge of the injection area and injection amount of SO₂ and H₂O. Additional model sensitivity tests with various injection amounts and latitude bands compared with several observational aerosol optical properties are detailed in Supplementary Note 1. Without the water injection, the SO₂only case has a very small sAOD in the first 2 weeks after the eruption, because SO₂ converts slowly to H₂SO₄ with a lifetime of ~1 month (Fig. 2). Both OMPS and the SO₂_H₂O case show almost immediate formation of a large amount of sulfate aerosol. OMPS LP sAOD retrieval during the first couple of days has large uncertainties when the volcanic clouds are optically thick and localized²⁹. The backscatter coefficient at visible wavelengths for the SO₂_H₂O case and CALIOP shows a similar peak value of 0.005 to 0.01 km⁻¹ sr⁻¹ (Supplementary Fig. 5). In addition, compared to the SO₂only case, sulfate particles in the SO₂_H₂O case doubled the sAOD in February because sulfate forms faster in the SO₂_H₂O case, and the more abundant particles coagulate to larger sizes. Also, sulfate particles swell to be a little larger because of the enhanced background water vapor (Supplementary Fig. 8). Generally, OMPS-LP observes a faster spreading of the plume to the northern hemisphere than is simulated (Fig. 3) and has higher optic values in the northern hemisphere in March

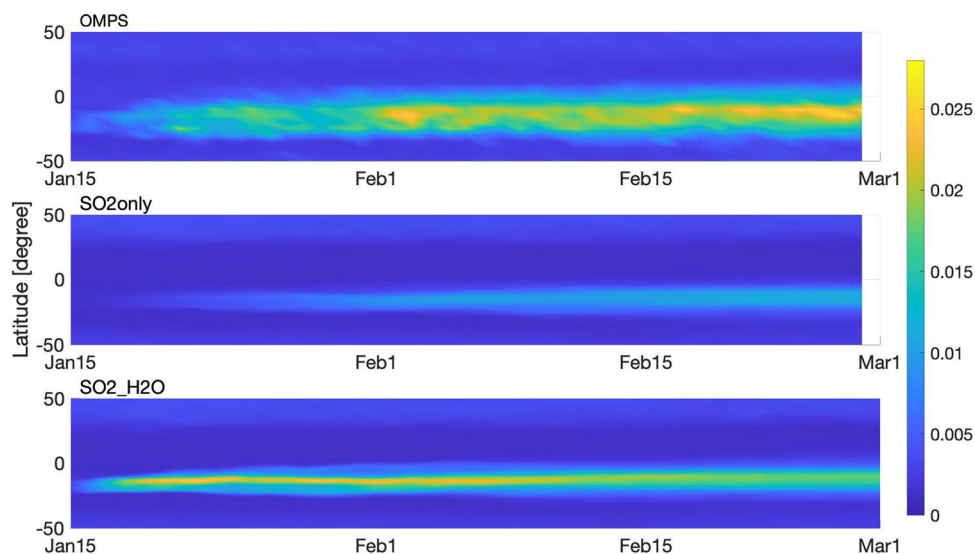


Fig. 3 The zonal mean column sAOD (stratospheric aerosol optical depth, background aerosol + volcanic aerosol). The top panel shows the OMPS LP (the Ozone Mapping and Profiling Suite Limb Profiler) at 997 nm. The middle and bottom panels show the simulated near-infrared sAOD (stratospheric aerosol optical depth) for cases without (the SO₂only case) and with the water injection (the SO₂_H₂O case).

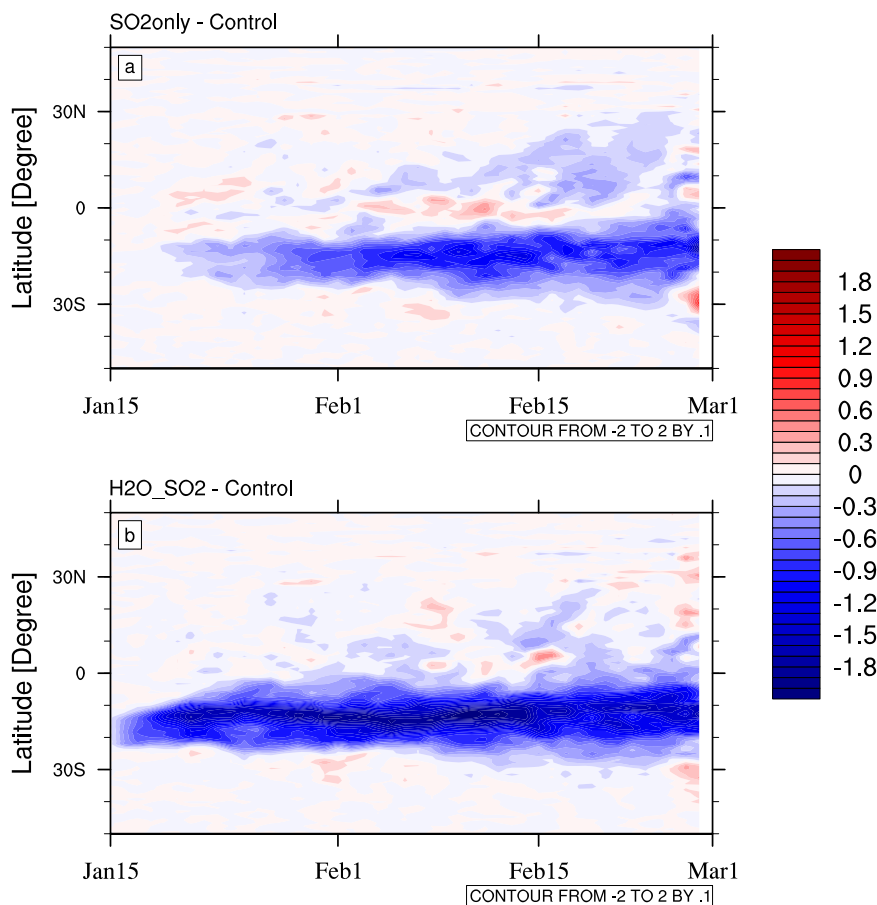


Fig. 4 The zonal average radiative effect (W m^{-2}) of the top of the atmosphere from January to March 2022. **a** The SO₂only case minus The control case; **b** the SO₂H₂O case minus the control case.

(Supplementary Fig. 9). Sellitto et al.³⁰ indicate the initial fast spreading of the HTHH aerosol plume is highly related to the strong cooling inside the plume. Our model is nudged to the observed meteorology, which does not capture this strong local cooling. Also, as we discuss in Result, the global model cannot reproduce the vertical wind shear as observed due to the limited spatial resolution. On March 1, the SO₂H₂O case and the OMPS observation are consistent regarding the vertical extent of the plume from 20 to 30 km, and the extension to 40°S (Supplementary Fig. 9).

Because of the increase in the burden of sulfate, the volcanic plume creates a negative radiative effect of about -1 to -2 W m^{-2} in the perturbed areas in January and February (Fig. 4). The global mean radiative effect at the top of the atmosphere in February is -0.13 W m^{-2} in the SO₂only case and -0.21 W m^{-2} in the SO₂H₂O case; the surface radiative effect is -0.16 W m^{-2} for the SO₂only case and -0.21 W m^{-2} for the SO₂H₂O case. These values are typical for middle-sized volcanic eruptions³¹. Even though the sAOD is approximately doubled in the SO₂H₂O case, it only results in slightly more negative radiative forcing due to enhanced positive radiative forcing of the enhanced water vapor^{32,33} in the SO₂H₂O case. Additional simulation with only H₂O injection shows the radiative effect from water is positive in the Southern hemisphere but is much smaller than that of the aerosol (Supplementary Fig. 10).

Persistent volcanic water vapor and sulfate may impact stratospheric ozone chemistry. Here we focus our study on the transport of volcanic water vapor and sulfate in the Southern

Hemisphere. We conduct three sets of 3-member ensemble simulations to explore the transport of volcanic water vapor and volcanic sulfate from January to October. The simulations are nudged to the observed meteorology until the end of March and then are free-running until October. Figure 5 shows that both H₂O and sulfur in the condensed phase are slowly transported to the south from January to May. After mid-June, the majority of H₂O and sulfur in the condensed phase reside between 30°S and 60°S. This is because the strong Antarctic vortex during June–July–August prevents volcanic materials from entering the polar cap. The black contours in Fig. 5 are the zonal wind showing the polar vortex starts to build up in April and remains through October between 50°S and 60°S. Figure 5c, d shows the percentage increase compared to the background levels of H₂O and sulfur in the condensed phase. Even though the majority of volcanic material is outside the polar vortex, we see a $\sim 10\%$ increase of sulfur in the condensed phase at 90°S starting from April and the mass of the sulfur in the condensed phase almost doubles in October. The sulfate aerosol provides extra surface area density (SAD) for heterogeneous reactions affecting ozone chemistry. On the other hand, water increases by about 20% at the edge of the vortex ($\sim 60^\circ\text{S}$) after June. However, due to polar stratospheric cloud formation and dehydration, the positive water anomaly inside the polar vortex does not pass the Student's *t*-test at a 90% significance level.

The simulations predict an increase in water vapor and aerosol surface area density (SAD) near the vortex. These changes are expected to impact polar ozone because heterogeneous reactions on polar stratospheric clouds and volcanic particles convert

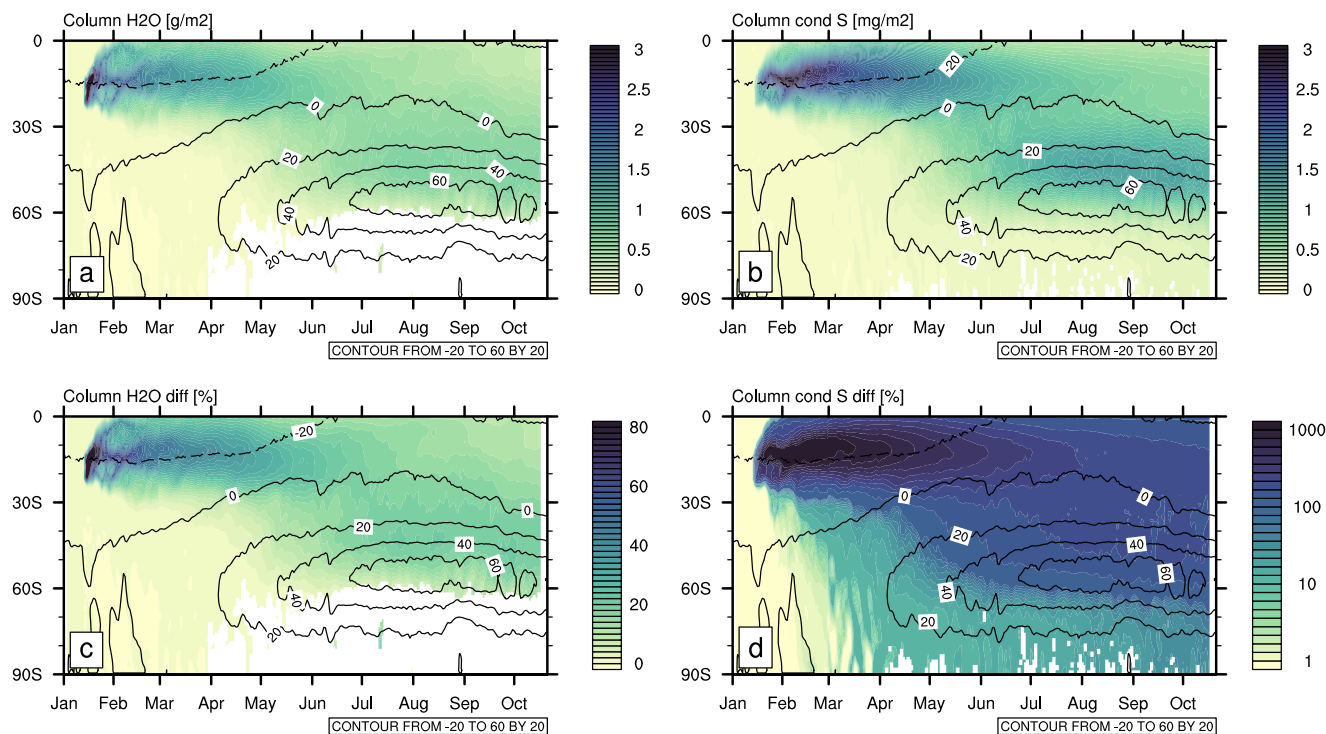


Fig. 5 The transport of volcanic H₂O (water) and sulfur in the condensed phase from January to October, 2022. **a, b** The transport of volcanic column H₂O and the mass density of volcanic column sulfur in the condensed phase towards the South Pole. “Column cond S” means the sulfur in the condensed phase. **c, d** Similar but plotted as the percentage increase relative to background H₂O and sulfur. After April 1, white areas mean the anomaly is not significant using the *t*-test at a 90% confidence level based on three ensemble members after April 1, 2022. The contours show the zonal wind showing the polar vortex from April to October at around 60°S.

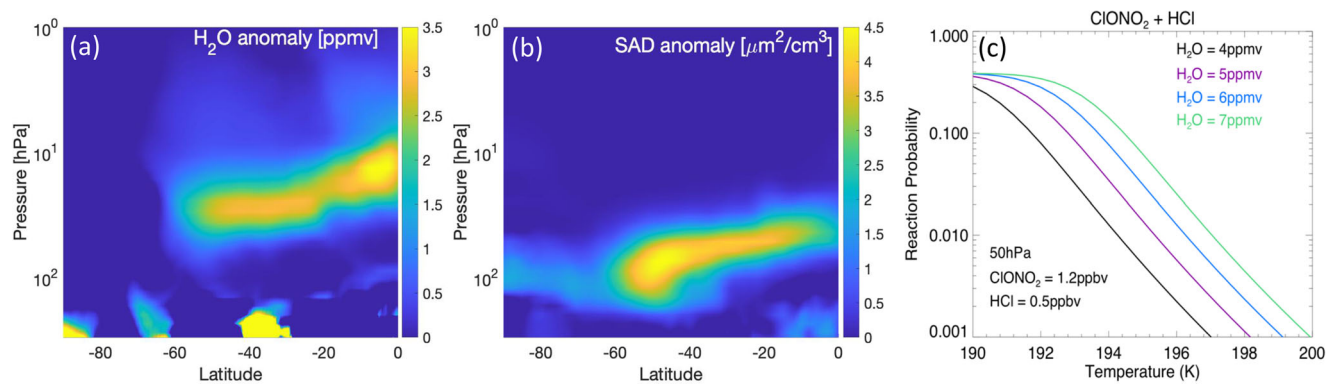


Fig. 6 The simulated water vapor, the aerosol SAD (surface area density) anomaly, and CIONO₂ + HCl (chlorine nitrate + hydrogen chloride) reaction probability. The simulated water vapor anomaly (a) and the aerosol SAD anomaly (b) in late September. These anomalies are calculated using the SO₂-H₂O case minus the control case. **c** The heterogeneous reaction rate as a function of water vapor assuming 0.1 μm particle size.

inactive chlorine (CIONO₂ and HCl) into photochemically active chlorine^{34,35}. Figure 6a, b shows that water increases by about 2–3 ppmv and SAD increases by about 2 to 4.5 μm² cm⁻³ near the edge of the vortex by the end of September. The SAD increases by about 1.5 μm² cm⁻³ inside the vortex at 100 hPa. Water vapor increases between 50 and 10 hPa, while the aerosol increase is between 150 and 30 hPa. This difference in altitude occurs because of aerosol sedimentation during transport. Figure 6c shows the HCl+CIONO₂ heterogeneous reaction rate³⁶ as a function of temperature for different amounts of water vapor. The reaction probability increases about one order of magnitude as we increase water by 3 ppmv above 194 K. Volcanic aerosols are well known to be a factor to impact ozone depletion by providing additional surface area and suppressing the NO_x cycle³⁷. The additional H₂O

changes in HTHH can impact the dynamics, HO_x chemical cycles, heterogeneous reaction rate, and the Polar Stratospheric Cloud formation (PSCs). The water vapor mixing ratio determines the vapor pressure of HNO₃ in the supercooled ternary solutions (Type Ib PSC) and impacts the ice PSC’s nucleation and growth. Both the direct impact and climate response caused by this eruption add complications to ozone assessment. Therefore, future studies will be conducted to explain how the volcanic H₂O and sulfate impact the 2022 Antarctic ozone depletion.

Discussion

The HTHH eruption provides a natural testbed to show how increased water vapor in the stratosphere can impact the Earth

system. This work demonstrates the importance of the water vapor injection on aerosol and aerosol-related chemistry using a state-of-the-art global climate model. The simulation shows that water vapor significantly shortens the SO₂ lifetime and doubles aerosol extinction relative to the simulation with only an SO₂ injection. The global radiative forcing of HTHH is on the order of -0.1 to -0.2 W m⁻² though it is about -1 to -2 W m⁻² from 30°S to 0° during the 2 months after the eruption. In the forecast simulation, volcanic water and sulfate persist near the polar vortex until at least October 2022. The model developed here provides opportunities for future studies on the climate impact, and effects on ozone, of HTHH eruption as it continues to evolve.

Methods

Model setup. We utilize the Community Earth System Model version 2 (CESM2) with the Whole Atmosphere Community Climate Model (WACCM)³⁸ using 70 layers extending upward to 140 km. The vertical resolution is about 1 to 1.5 km in the stratosphere. The model is fully coupled to an interactive ocean, sea-ice, and land. The ocean and sea-ice are initialized on January 3 with output from a stand-alone ocean model forced by atmospheric state fields and fluxes from the Japanese 55-year Reanalysis³⁹. Likewise, the land is initialized with output from a stand-alone land model forced with atmospheric data from the National Center for Environmental Prediction Climate Forecast System, version 2. These are the same initializations that were used in the subseasonal-to-seasonal project⁴⁰. The atmosphere is initialized from a transient WACCM simulation³⁸. Between January 3 and March 30, 2022, the atmospheric component is nudged to GEOS5 meteorological analysis⁴¹ with a 12-h relaxation using 3-h meteorology⁴². After April 1, three ensemble members with a fully interactive atmosphere and ocean are continued into the future until the end of October. The three ensemble members differ in the last date of nudging (namely March 29, 30, and 31). We conducted three sets of ensemble members: the control case without SO₂ or H₂O; the SO₂only case with only SO₂ injection; and the SO₂H₂O case with both SO₂ and H₂O injection. We conduct a H₂Oonly case with only H₂O injection to investigate the radiative impact from H₂O.

The SO₂ injection amount is based on the TROPOMI and OMPS Nadir Mapper (NM) SO₂⁴³ reported at <https://so2.gsfc.nasa.gov/>. We tune the SO₂ injection vertical distributions based on comparisons between the simulated sulfate aerosol and OMPS LP aerosol extinction in March (i.e., Supplementary Fig. 9). We tune the H₂O injection amount and vertical distribution mainly to retain enough H₂O between 10 and 50 hPa as seen by MLS in Feb, March, and April (i.e., Fig. 1a). MLS also sees a small amount of water between 10 to 1 hPa in those days⁵. We inject 0.42 Tg of SO₂ and 150 Tg of H₂O from 4 UTC to 10 UTC on January 15, 2022 (ignoring the small eruption that occurred on January 13, 2022. Note that this small eruption also put ice into the lower stratosphere, up to 20 km). The vertical distribution of SO₂ is 0.3 Tg from 20 to 22 km and 0.12 Tg from 22 to 28 km with constant number densities in these layers. The vertical distribution of H₂O is 103 Tg from 25.5 to 27 km, 42 Tg from 27 to 30 km, and 5 Tg from 30 to 35 km with constant concentration. We inject the plume into an area of $\sim 6 \times 10^5$ km² between 22°S–14°S and 182°E–186°E, which is about three times larger than the anvil size observed by NOAA's Geostationary Operational Environmental Satellite 17 on January 15, 2022. This is because the MLS observes H₂O occupying ~ 10 -degree latitude bands on January 15⁵. Also, the global model cannot spread the plume as fast as observed as we discuss in Result. We have not considered ash injection since satellite observations (e.g., OMPS measured low UV Aerosol Index) do not show evidence of notable ash persisting for a long time. CALIOP sees that the majority of the high backscatter coefficient above 20 km correlates with low depolarization indicating the composition is mainly spherical sulfate particles. The Light Optical Aerosol Counter (LOAC) measurements at Reunion island (21.1°S, 55.3°E) on January 23 and January 26 mainly see submicron particles indicating no large volcanic ash or other large (>1 μm) volcanic particles present. Supplementary Note 1 presents several other model simulations with a larger SO₂ injection amount (0.84 Tg) or a wider injection band (20-degree latitude band) for both SO₂H₂O and SO₂only cases as sensitivity tests.

For ice cloud formation, we modified the nucleation parameterization to allow both homogeneous freezing and heterogeneous nucleation to occur in the stratosphere when temperatures are cold (<−40 °C).

Observations. The MLS instrument onboard the EOS Aura satellite was launched into a near-polar sun-synchronous orbit in 2004 and measures atmospheric composition, temperature, humidity, and cloud ice. After the HTHH eruption, MLS detected enhanced water vapor. Here we use MLS version 4 quality screened data⁶ and do not use MLS ice water content as recommended by Millán et al.⁵.

The OMPS Limb Profiler (LP)⁴⁴ data have been processed to create an aerosol extinction coefficient product from measurements of the limb scattered solar radiation at six wavelengths. The sensor employs three vertical slits separated horizontally. This work uses the version 2.0 OMPS aerosol extinction coefficient product at 997 nm wavelength²⁸ with relative accuracies and precisions close to

15%. We use the center slit aerosol retrieval because it has the most accurate radiometric calibration and stray light corrections⁴⁵.

SO₂ mass estimates from OMPS-NM are based on the NASA standard SNPP/OMPS SO₂ vertical column density (VCD) product, retrieved using a principal component analysis (PCA) spectral fitting algorithm⁴³ assuming a fixed a priori profile centered at 18 km altitude. The estimated uncertainty of $\sim 35\%$ (error bar in Fig. 2) reflects potential errors that can be caused by the highly unusual injection height and the large amounts of aerosols and ice particles for the HTHH eruption. For OMPS data, the detection limit is based on the 1-sigma noise level of OMPS SO₂ retrievals of ~ 0.1 DU over background, SO₂-free areas. Any pixels with retrieved SO₂ < 0.2 DU, we consider to be noise and for volcanic SO₂ mass calculation those pixels are excluded (i.e., we calculate the total mass by summing up SO₂ mass from all the OMPS pixels with SO₂ \geq 0.2 DU). In order to compare the modeled SO₂ with observations as shown in Fig. 2, we apply a similar method as the observation by excluding modeled grid boxes with SO₂ < 0.2 DU. This way, the model-based SO₂ mass is calculated in a more consistent way with OMPS-based estimate. The comparisons between the modeled SO₂ and OMPS-NM SO₂ retrieval without applying detection limit (Supplementary Fig. 11) also agree within the error bars.

Data availability

The main data generated during this study are available at (<https://osf.io/6ZXFV/>) with a permanent doi 10.17605/OSF.IO/6ZXFV. OMPS-LP data are available at https://disc.gsfc.nasa.gov/datasets/OMPS_NPP_LP_L2_O3_DAILY_2/summary. CALIPSO data are available at <https://asdc.larc.nasa.gov/project/CALIPSO>. SAGE III/ISS data are available at <https://asdc.larc.nasa.gov/project/SAGE%20III-ISS>. The TROPOMI and OMPS-NM SO₂ data are available at <https://so2.gsfc.nasa.gov/>.

Code availability

The CESM2 model is available on the CESM trunk to any registered user at www.cesm.ucar.edu.

Received: 30 May 2022; Accepted: 7 October 2022;

Published online: 22 October 2022

References

- Carr, J. L., Horváth, Á., Wu, D. L. & Friberg, M. D. Stereo plume height and motion retrievals for the record-setting Hunga Tonga-Hunga Ha'apai eruption of 15 January 2022. *Geophys. Res. Lett.* e2022GL098131, <https://doi.org/10.1029/2022GL098131> (2022).
- Proud, S. R., Prata, A. & Schmauss, S. The January 2022 eruption of Hunga Tonga-Hunga Ha'apai volcano reached the mesosphere. *Earth Space Sci. Open Arch.* <https://doi.org/10.1002/essoar.10511092.1> (2022).
- Yuen, D. A. et al. Under the surface: Pressure-induced planetary-scale waves, volcanic lightning, and gaseous clouds caused by the submarine eruption of Hunga Tonga-Hunga Ha'apai volcano. *Earthq. Res. Adv.* 100134, <https://doi.org/10.1016/j.eqrea.2022.100134> (2022).
- Xu, J., Li, D., Bai, Z., Tao, M. & Bian, J. Large amounts of water vapor were injected into the stratosphere by the Hunga Tonga-Hunga Ha'apai volcano eruption. *Atmosphere* 13, <https://doi.org/10.3390/atmos13060912> (2022).
- Millán, L. et al. The Hunga Tonga-Hunga Ha'apai hydration of the stratosphere. *Geophys. Res. Lett.* 49, <https://doi.org/10.1029/2022GL099381> (2022).
- Livesey, N. J. et al. Version 4.2x Level 2 and 3 data quality and description document (Tech. Rep. No. JPL D-33509 Rev. E) (2020).
- Winker, D. M., Hunt, W. H. & McGill, M. J. Initial performance assessment of CALIOP. *Geophys. Res. Lett.* 34, <https://doi.org/10.1029/2007GL030135> (2007).
- Guo, S., Rose, W. I., Bluth, G. J. S. & Watson, I. M. Particles in the great Pinatubo volcanic cloud of June 1991: the role of ice. *Geochem. Geophys. Geosys.* 5, <https://doi.org/10.1029/2003GC000655> (2004).
- Mills, M. J. et al. Radiative and chemical response to interactive stratospheric sulfate aerosols in fully coupled CESM1(WACCM). *J. Geophys. Res. Atmos.* 122, 13,061–13,078 (2017).
- Dvortsov, V. L. & Solomon, S. Response of the stratospheric temperatures and ozone to past and future increases in stratospheric humidity. *J. Geophys. Res. Atmos.* 106, 7505–7514 (2001).
- Hofmann, D. & Oltmans, S. The effect of stratospheric water vapor on the heterogeneous reaction rate of ClONO₂ and H₂O for sulfuric acid aerosol. *Geophys. Res. Lett.* 19, 2211–2214 (1992).
- Solomon, S. Stratospheric ozone depletion: a review of concepts and history. *Rev. Geophys.* 37, 275–316 (1999).

13. Solomon, S. et al. Emergence of healing in the Antarctic ozone layer. *Science* **353**, 269–274 (2016).
14. Zhu, Y. et al. Stratospheric aerosols, Polar Stratospheric Clouds, and polar ozone depletion after the Mount Calbuco eruption in 2015. *J. Geophys. Res. Atmos.* **123**, 12,308–12,331 (2018).
15. LeGrande, A. N., Tsigaridis, K. & Bauer, S. E. Role of atmospheric chemistry in the climate impacts of stratospheric volcanic injections. *Nat. Geosci.* **9**, 652–655 (2016).
16. de F. Forster, P. M. & Shine, K. P. Stratospheric water vapour changes as a possible contributor to observed stratospheric cooling. *Geophys. Res. Lett.* **26**, 3309–3312 (1999).
17. Shindell, D. T. Climate and ozone response to increased stratospheric water vapor. *Geophys. Res. Lett.* **28**, 1551–1554 (2001).
18. Smith, C. A., Haigh, J. D. & Toumi, R. Radiative forcing due to trends in stratospheric water vapour. *Geophys. Res. Lett.* **28**, 179–182 (2001).
19. Solomon, S. et al. Contributions of stratospheric water vapor to decadal changes in the rate of global warming. *Science* **327**, 1219–1223 (2010).
20. Ploeger, F. et al. The stratospheric Brewer–Dobson circulation inferred from age of air in the ERA5 reanalysis. *Atmos. Chem. Phys.* **21**, 8393–8412 (2021).
21. Zhu, Y. et al. Persisting volcanic ash particles impact stratospheric SO₂ lifetime and aerosol optical properties. *Nat. Commun.* **11**, 4526 (2020).
22. Clyne, M. et al. Model physics and chemistry causing intermodel disagreement within the VolMIP-Tambora Interactive Stratospheric Aerosol ensemble. *Atmos. Chem. Phys.* **21**, 3317–3343 (2021).
23. Bekki, S. Oxidation of volcanic SO₂: a sink for stratospheric OH and H₂O. *Geophys. Res. Lett.* **22**, 913–916 (1995).
24. Pinto, J. P., Turco, R. P. & Toon, O. B. Self-limiting physical and chemical effects in volcanic eruption clouds. *J. Geophys. Res. Atmos.* **94**, 11165–11174 (1989).
25. Savarino, J., Bekki, S., Cole-Dai, J. & Thiemens, M. H. Evidence from sulfate mass independent oxygen isotopic compositions of dramatic changes in atmospheric oxidation following massive volcanic eruptions. *J. Geophys. Res. Atmos.* **108**, 4671 (2003).
26. Theys, N. et al. Sulfur dioxide retrievals from TROPOMI onboard Sentinel-5 Precursor: algorithm theoretical basis. *Atmos. Meas. Tech.* **10**, 119–153 (2017).
27. Clegg, M. & Abbatt, D. Uptake of gas-phase SO₂ and H₂O₂ by ice surfaces: dependence on partial pressure, temperature, and surface acidity. *J. Phys. Chem. A* **105**, 6630–6636 (2001).
28. Taha, G. et al. OMPS LP Version 2.0 multi-wavelength aerosol extinction coefficient retrieval algorithm. *Atmos. Meas. Tech.* **14**, 1015–1036 (2021).
29. DeLand, M. Readme document for the Suomi-NPP OPMS LP L2 AER675 Daily product (2019).
30. Sellitto, P. et al. The unexpected radiative impact of the Hunga Tonga eruption of January 15th, 2022. <https://doi.org/10.21203/rs.3.rs-1562573/v1> (2022).
31. Schmidt, A. et al. Volcanic radiative forcing from 1979 to 2015. *J. Geophys. Res. Atmos.* **123**, 12491–12508 (2018).
32. Huang, Y. On the longwave climate feedbacks. *J. Clim.* **26**, 7603–7610 (2013).
33. Dessler, A., Schoeberl, M., Wang, T., Davis, S. & Rosenlof, K. Stratospheric water vapor feedback. *Proc. Natl Acad. Sci. USA* **110**, 18087–18091 (2013).
34. Solomon, S., Garcia, R. R., Rowland, F. S. & Wuebbles, D. J. On the depletion of Antarctic ozone. *Nature* **321**, 755–758 (1986).
35. Solomon, S. et al. The role of aerosol variations in anthropogenic ozone depletion at northern midlatitudes. *J. Geophys. Res. Atmos.* **101**, 6713–6727 (1996).
36. Shi, Q., Jayne, J., Kolb, C., Worsnop, D. & Davidovits, P. Kinetic model for reaction of ClONO₂ with H₂O and HCl and HOCl with HCl in sulfuric acid solutions. *J. Geophys. Res. Atmos.* **106**, 24259–24274 (2001).
37. Tie, X. & Brasseur, G. The response of stratospheric ozone to volcanic eruptions: sensitivity to atmospheric chlorine loading. *Geophys. Res. Lett.* **22**, 3035–3038 (1995).
38. Gettelman, A. et al. The whole atmosphere community climate model version 6 (WACCM6). *J. Geophys. Res. Atmos.* **124**, 12380–12403 (2019).
39. Tsujino, H. et al. JRA-55 based surface dataset for driving ocean–sea-ice models (JRA55-do). *Ocean Modell.* **130**, 79–139 (2018).
40. Richter, J. H. et al. Subseasonal Earth system prediction with CESM2. *Weather Forecast.* <https://doi.org/10.1175/WAF-D-21-0163.1> (2022).
41. Rienecker, M. M. et al. *The GEOS-5 Data Assimilation System: Documentation of Versions 5.0.1, 5.1.0, and 5.2.0* (2008).
42. Davis, N. A., Callaghan, P., Simpson, I. R. & Tilmes, S. Specified dynamics scheme impacts on wave-mean flow dynamics, convection, and tracer transport in CESM2 (WACCM6). *Atmos. Chem. Phys.* **22**, 197–214 (2022).
43. Li, C. et al. New-generation NASA Aura Ozone Monitoring Instrument (OMI) volcanic SO₂ dataset: algorithm description, initial results, and continuation with the Suomi-NPP Ozone Mapping and Profiler Suite (OMPS). *Atmos. Meas. Tech.* **10**, 445–458 (2017).
44. Flynn, L. E., Seftor, C. J., Larsen, J. C. & Xu, P. In *Earth Science Satellite Remote Sensing* 279–296 (Springer, 2006).
45. Jaross, G. et al. OMPS Limb Profiler instrument performance assessment. *J. Geophys. Res. Atmos.* **119**, 4399–4412 (2014).

Acknowledgements

The work at the University of Colorado Boulder was supported by NASA grant 80NSSC19K1276. This project received funding from NOAA’s Earth Radiation Budget (ERB) Initiative (CPO #03-01-07-001). This research was supported in part by NOAA cooperative agreements NA17OAR4320101 and NA22OAR4320151. C.K. acknowledges the support by LABEX-VOLTAIRE (ANR-10-LABEX-100-01). P.Y. is supported by the National Natural Science Foundation of China (42175089, 42121004). Development, analysis, and maintenance of the OMPS-NM SO₂ product are supported by the NASA Earth Science TASNPP (grant # 80NSSC18K0688) and SNPPSP (grant # 80NSSC22K0158) programs. Work at the Jet Propulsion Laboratory, California Institute of Technology, was carried out under a contract with the National Aeronautics and Space Administration (80NM0018D0004). X.W. is supported by the NSF via the NCAR’s Advanced Study Program Postdoctoral Fellowship. We thank the discussions at the SSiRC volcano forum led by Dr. Jean-Paul Vernier. We thank Dr. Nathaniel Livesey and Dr. Michelle Santee from the NASA MLS team, Dr. Margaret Tolbert from CU Boulder, Dr. Jadwiga Richter, Dr. William Randel and Dr. Mijeong Park from NCAR, Dr. Peter Colarco from NASA Goddard, Dr. Michael Pitts from NASA Langley, Dr. Ming Deng from LASP, and Dr. Tao Wang from NASA JPL, for their valuable input. NCAR’s Community Earth System Model project is supported primarily by the National Science Foundation. This material is based upon work supported by the National Center for Atmospheric Research, which is a major facility sponsored by the NSF under Cooperative Agreement No. 1852977. Computing and data storage resources, including the Cheyenne supercomputer (doi:10.5065/D6RX99HX), were provided by the Computational and Information Systems Laboratory (CISL) at NCAR.

Author contributions

O.B.T., C.G.B., S.T., M.J.M., K.H.R., and Y.Z. discussed the hypothesis. X.W., V.L.H., L.M., and Y.Z. analyzed the MLS H₂O data and simulations. G.T. and C.K. provided aerosol data and participated the aerosol data analysis. D.K. examined the sensitivity of the stratospheric H₂O abundance on the ClONO₂ + HCl reaction probability (Fig. 6c). C.G.B., S.T., M.J.M., S.G., and Y.Z. participated in the model development, preparation, and conducted simulations. R.P., P.Y., and Y.Z. analyzed the radiative impact. M.A. and T.D. interpreted CALIPSO volcanic plume observations. C.L. and N.K. provided the OMPS-NM data. All the authors wrote the manuscript and edited the manuscript.

Competing interests

The authors declare no competing interests.

Additional information

Supplementary information The online version contains supplementary material available at <https://doi.org/10.1038/s43247-022-00580-w>.

Correspondence and requests for materials should be addressed to Yunqian Zhu.

Peer review information *Communications Earth & Environment* thanks Sandip Dhomse, Chris Sioris and the other, anonymous, reviewer(s) for their contribution to the peer review of this work. Primary Handling Editors: Emma Liu and Clare Davis.

Reprints and permission information is available at <http://www.nature.com/reprints>

Publisher’s note Springer Nature remains neutral with regard to jurisdictional claims in published maps and institutional affiliations.



Open Access This article is licensed under a Creative Commons Attribution 4.0 International License, which permits use, sharing, adaptation, distribution and reproduction in any medium or format, as long as you give appropriate credit to the original author(s) and the source, provide a link to the Creative Commons license, and indicate if changes were made. The images or other third party material in this article are included in the article’s Creative Commons license, unless indicated otherwise in a credit line to the material. If material is not included in the article’s Creative Commons license and your intended use is not permitted by statutory regulation or exceeds the permitted use, you will need to obtain permission directly from the copyright holder. To view a copy of this license, visit <http://creativecommons.org/licenses/by/4.0/>.

© The Author(s) 2022